TUDelft

Delft University of Technology

High-Performance Motion Control of the METIS Cold Chopper Mechanism

Huisman, Robert; Paalvast, Sander; Brandl, Bernhard R.; Van Den Dool, Teun; Eggens, Martin; Janssen, Huub; Aitink-Kroes, Gabby; Molster, Frank; Teuwen, Maurice; Venema, Lars

Important note
To cite this publication, please use the final published version (if applicable).
Please check the document version above.

1

High performance motion control of the METIS Cold Chopper Mechanism

R. Huisman, S. Paalvast, B. Brandl, T.C. van den Dool, M. Eggens, H. Janssen, G. Aitink-Kroes, F. Molster, M. Teuwen, L. Venema and B. Jayawardhana

Abstract—We present the main results of the performance test campaign of the METIS Cold Chopper Demonstrator (MCCD). This tip/tilt mirror, which operates at a temperature of 77K, is one of the critical components in the Mid-Infrared E-ELT Imager and Spectrograph (METIS) for the European Extremely Large Telescope (E-ELT). The performance requirements of the MCCD relate to the field of fast and very accurate reference tracking. We discuss the applicability of different high performance motion control strategies and describe the control synthesis of a repetitive and of a novel hybrid controller. We identified the presence of non linearities in the plant, which limits the performance of the hybrid controller. The repetitive controller shows very promising results and can handle the non linearities in the system. This experimental phase concludes the MCCD program, which was initiated to verify the feasibility of a high performance cryogenic tip/tilt mirror at an early stage in the METIS development. Because of the very promising test results, no significant changes to the hardware will be implemented. We believe that minor adjustments will suffice to meet all requirements of the final hardware after integration with the METIS instrument.

Index Terms—high performance motion control, hybrid control, repetitive control, control synthesis, hysteresis, tip/tilt mechanism

I. INTRODUCTION

The METIS Cold Chopper (MCC) mechanism is one of the critical components in the Mid-Infrared E-ELT Imager and Spectrograph (METIS) [1] for the European Extremely Large Telescope (E-ELT) [2]. With its 39m dish, the E-ELT will be the largest optical/infrared telescope ever. The E-ELT will see first light in 2024 and is being developed by the European Southern Observatory (ESO).

R. Huisman and M. Eggens are with SRON Netherlands Institute for Space Research, Postbus 800, 9700AV Groningen, The Netherlands. (e-mail: r.huisman@sron.nl)

H. Janssen, M. Teuwen, and S. Paalvast are with Janssen Precision Engineering, Aziëlaan 12, 6199AG Maastricht-Airport, The Netherlands (www.jpe.nl)

B. Brandl is with Leiden Observatory, Leiden University, P.O. Box 9513, 2300RA Leiden, The Netherlands and TU Delft, Faculty of Aerospace Engineering, Kluyverweg 1, 2629HS Delft, The Netherlands

T.C. van den Dool is with TNO opto-mechatronics, Stieltjesweg 1, 2628CK Delft, The Netherlands. (e-mail: teun.vandendool@tno.nl)

G. Aitink-Kroes is with NOVA - optical/infrared instrumentation group, Oude Hoogeveensedijk 4, 7991PD Dwingeloo, The Netherlands

F. Molster is with Leidse instrumentmakers School, Einsteinweg 61, 2333CC Leiden, The Netherlands and NOVA, Niels Bohrweg 2, 2333CA Leiden, The Netherlands

L. Venema is with ASTRON, P.O. Box 2, 7990AA Dwingeloo, The Netherlands

B. Jayawardhana is with the Faculty of Mathematics and Natural Sciences, the University of Groningen, 9747AG Groningen, The Netherlands. (e-mail: b.jayawardhana@rug.nl)

METIS will be one of the first three scientific instruments on the E-ELT, covering the thermal infrared wavelength range. At these wavelengths, very accurate subtraction of the spatially and temporally varying background is essential. This is usually done by beam chopping, i.e., alternating the optical beam between science target and a reference location on the nearby sky at a frequency of a few Herz. While the beam chopping is traditionally done by the telescope's secondary mirror, this option does not exist for the E-ELT and an alternative solution within METIS had to be found.

This work is part of the MCC demonstrator (MCCD) project, which was initiated to show the feasibility of a high performance chopping mirror inside a cryogenic instrument at an early stage in the METIS development. The MCC is a tip/tilt mirror at the pupil position of METIS. Tilting the MCC in two dimensions moves the orientation of the telescope beam on the sky without having to move the telescope.

Different chopping and scanning strategies can be considered [3]. The focus here is on the so called chopping or beam switching technique, where the mirror quickly chops between two or more exactly reproducible mirror positions. From differential measurements the sky background and detector noise can be derived and subtracted from the image which contains the source.

Several challenging performance requirements drive the design of both hardware and control of the MCC (see Table VII of Section IV). Most notably are the requirements for short beam switching times (i.e., high observing efficiency with small overheads, which requires short settling times) and very accurate positional repeatability (which is required for sharp images in co-added, long term exposures). Meeting these requirements simultaneously is very challenging from a control perspective, which is related to the field of high performance motion control.

Different control strategies are available for high performance motion control of nano positioning mechanisms. What these techniques generally have in common is the application of a feedforward (FF) signal for fast stepping, typically but not necessarily in parallel with a feedback controller for noise reduction and robustness. Although the design of this FF signal is usually based on the available knowledge of the plant dynamics (model based approach), the details about the generation of the FF signal [4] [5] and the shaping of the reference profile [6] [7] can vary a lot.

When reference profiles of a repetitive nature are applied, as for this application, one can also consider the use of a repetitive controller [8] [9]. Different from the model based

approach, the repetitive loop generates the FF signal by learning with every repetition.

We developed a hybrid control strategy [10], [11] which applies a FF input in open loop during the step, to avoid possible negative effects of the closed loop controller because of its limited bandwidth w.r.t. the frequency content of the reference profile as discussed in [10], [12], and switches to closed loop during the observation periods. The method involves resetting, memorizing and switching between different sets of control states at fixed moments during an observation. Resetting of the control states is similar to reset control [13] and impulsive control [14], where the state of a feedback controller is subject to sudden changes dictated by the reference profile or the tracking error. A clear distinction with our method however is the definition of the initial control states at the start of every observation period and that we perform the step in open loop. We compare the experimental results applying this strategy with that of a repetitive controller and discuss the different issues related to both methods.

In Section II we describe in detail the system identification of the hardware, which revealed the presence of hysteresis in the system. The applied control strategies are described in Section III and the experimental results are given in Section IV. We discuss some of the issues regarding the implementation of the control strategy in Section V and the conclusions of the test campaign are given in Section VI.

II. SYSTEM IDENTIFICATION

A. Hardware and test setup

For details about the MCCD mechatronic design the reader is referred to [15]. Here we summarize the key mechatronic elements of the mechanism and describe the experimental test setup. Details about the dynamical behaviour of the system are given in Section *II.B*.

A schematic overview of the MCCD mechanism, which is designed to operate in cryogenic conditions, is shown in Fig. 1. It has 3 Degrees of Freedom (DoF), which composes of rotation around the x and y-axis (tip/tilt) and translation along the z-axis. The triangular support structure with the circular mirror body is supported by 3 monolithic struts with elastic hinges to constrain the 3 undesired DoF's without introducing backlash or friction. Displacements are measured by 3 Attocube position sensors (type: FPS3010) based on the principle of laser interferometry and actuation is provided by 3 voice coil actuators. These voice coil actuators were specially developed for the MCCD. In the design the back iron is detached from the permanent magnet. It is fixed to the base structure which limits the amount of moving mass (magnet only) of the actuator and therefore considerably reduces the moment of inertia of the mirror body.

The mechanism dynamics (inertia, spring constant and damping) are designed to be rotationally symmetric. The multiple-input multiple-output (MIMO) system is converted to three decoupled single-input single-output (SISO) systems

by applying the following matrix transformations.

$$\begin{bmatrix} z \\ \theta_x \\ \theta_y \end{bmatrix} = \begin{bmatrix} \frac{1}{3} & \frac{1}{3} & \frac{1}{3} \\ 0 & \frac{1}{\sqrt{3}r_s} & -\frac{1}{\sqrt{3}r_s} \\ \frac{2}{3r_s} & -\frac{1}{3r_s} & -\frac{1}{3r_s} \end{bmatrix} \begin{bmatrix} z_1 \\ z_2 \\ z_3 \end{bmatrix} \tag{1}$$

$$\begin{bmatrix} F_1 \\ F_2 \\ F_3 \end{bmatrix} = \begin{bmatrix} \frac{1}{3} & 0 & \frac{-2}{3r_f} \\ \frac{1}{3} & \frac{1}{\sqrt{3}r_f} & \frac{1}{3r_f} \\ \frac{1}{3} & \frac{-1}{\sqrt{3}r_f} & \frac{1}{3r_f} \end{bmatrix} \begin{bmatrix} F_z \\ M_{\theta_x} \\ M_{\theta_y} \end{bmatrix} \tag{2}$$

(1) relates the three sensor readouts (z_1, z_2 and z_3) to the three DoF's of the system, where r_s is the radial distance of the sensors to the heart of the mirror. (2) converts the control inputs (F_z, M_{θ_x} and M_{θ_y}) for the different DoF's, to the individual force inputs (F_1, F_2 and F_3) of the actuators. Here r_f is the radial distance of the actuators to the heart of the mirror.

The experimental setup is sketched in Fig. 2. Tests are performed in a cryostat at an operating temperature of 77K. The sensor electronics are placed outside the cryostat. The optical measurement signal is guided to the MCCD hardware by 3 glass fibers. Calibration of the 2 DoF rotational motion is performed using a theodolite. The Matlab xPC target platform is used to implement the digital controller (designed in Matlab Simulink using a host PC) on a target machine. The system runs at a sampling rate of 10 kHz.
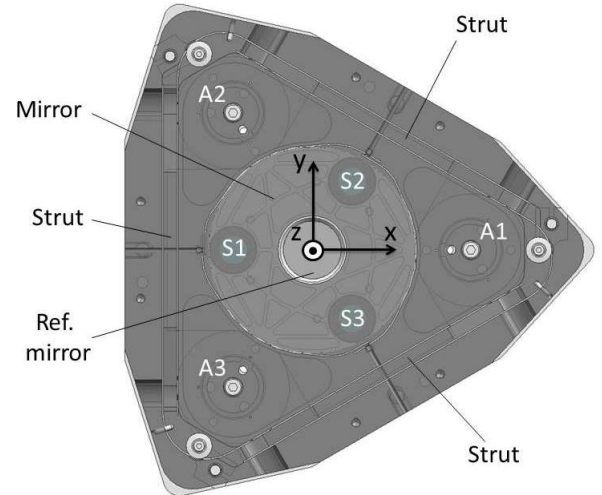

Fig. 1. Schematic overview of the MCCD mechanism. Triangular support structure with circular mirror body is made transparent to show the location of the sensors (S1, S2 and S3) and actuators (A1, A2 and A3). The fixed reference mirror at the heart of the structure is used for test purposes only and will not be part of the final MCC. Coordinate system is also indicated. Design by Janssen Precision Engineering (JPE)

B. Plant dynamics

System identification is performed by the method of frequency analysis. The experimental data is generated applying a high resolution sinesweep over the frequency regime from 5Hz to 2kHz and fitting the steady state response of the system (input and output) to a sine profile. This provides us with the phase shift and gain information required to generate the bode
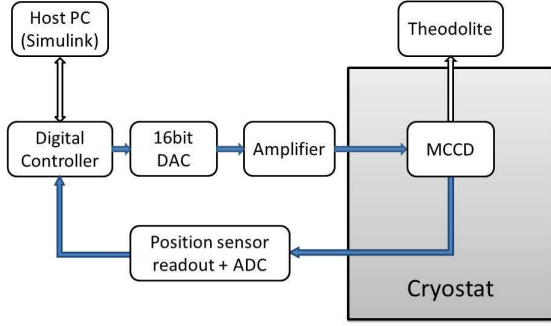
Fig. 2. Block diagram showing the general building blocks of the experimental setup. The MCCD is placed in a cryostat and tests are performed at an operating temperature of 77K.

plot. We only use the magnitude plot for model fitting because of the limited accuracy of the phase information.

Fig. 3 shows the bode magnitude plot of the open loop plant for θ_x. The dominant resonance frequencies of the mechanism are clearly visible. Table I gives these dominant resonance frequencies and compares them to the results from a detailed Finite Element Analysis (FEA) [16].

The resonant behaviour at approximately 500Hz cannot be explained by the mechanism dynamics. The same is true for a small, but relevant resonance at 125Hz. These resonances do not show up in the FEA and, despite the rotational symmetry of the MCCD, are not present in the θ_y dynamics. They are believed to originate from the test setup e.g., the cryostat , whose structural dynamics are not symmetrical w.r.t. the introduced forces as a result of θ_x or θ_y-rotation.

Due to the influence of the cryostat, we consider a non collocated lumped mass system as shown in Fig. 4 to describe the θ_x-dynamics. This results in an 8th-order system with 5 stable zeros, i.e. 2 complex conjugated pairs close to respectively the 125Hz and the 500Hz resonance and one zero at high frequency. Based on this system, we model the θ_x-dynamics including the dominant resonance at 29.6Hz, a skew notch at 125Hz and at 487Hz and a broad resonance at 1440Hz (to account for the two sharp resonances between 1.4 and 1.5kHz). The high frequency zero has very limited influence on the system response and we choose to ignore this in our system model.

The θ_y-dynamics are modelled as a 4th-order plant excluding the two resonances related to the cryostat. Finally, the z-dynamics are less critical and can be approximated by a 2nd-order plant.

Using the transfer function given by:

$$P(s) = \frac{a_n s^n + a_{n-1}s^{n-1} + ... + a_1 s + a_0}{b_n s^n + b_{n-1}s^{n-1} + ... + b_1 s + b_0} \quad (3)$$

where $a_n,...,a_0,b_n,...,b_0$ are coefficients to be fitted, the final system models for the different DoF's are given in Table II.

Comparison of the simulated step response with experimental data shows a good match for the 1 mrad chop range for which the identification has been performed (see for example Fig. 7 (0° offset result)).

A detailed system model, including the weak resonance at

TABLE I
DOMINANT RESONANCES OF MCCD FOR θ_x ORIENTATION. EXPERIMENTAL AND FEA RESULTS GENERATED USING CREO SIMULATE AND CREO PARAMETRIC SOFTWARE

Measured	FEA
29.6 Hz	29.0 Hz
1405.0 Hz	1443.1 Hz
1470.0 Hz	1491.0 Hz

TABLE II
LAPLACE TRANSFORM COEFFICIENTS FOR ALL 3 DoF'S. THE GIVEN COEFFICIENTS ARE RELATED TO THE STANDARD TRANSFER FUNCTION GIVEN IN (3). THESE ARE ROUNDED VALUES TAKEN FROM THE 64BIT FLOATING POINT NUMBERS PROVIDED BY MATLAB.

n	P_{θ_x} a_n	P_{θ_x} b_n	P_{θ_y} a_n	P_{θ_y} b_n	P_z a_n	P_z b_n
8	-	1	-	-	-	-
7	-	178.5	-	-	-	-
6	-	1.68×10⁸	-	-	-	-
5	-	1.45×10¹⁰	-	-	-	-
4	5.11×10¹⁴	1.60×10¹⁵	-	1	-	-
3	3.72×10¹⁶	4.85×10¹⁶	-	77.80	-	-
2	4.95×10²¹	9.51×10²⁰	-	8.19×10⁷	-	1
1	1.00×10²³	9.71×10²¹	-	7.77×10⁸	-	10.48
0	2.77×10²⁷	3.09×10²⁵	2.53×10¹⁴	2.76×10¹²	1.01×10⁴	1.59×10⁴

125Hz is required for an accurate FF design. This is discussed in more detail in Section III-A.

C. Non linear behaviour

The experimental results revealed the presence of non negligible non linearities in the system. This is shown in Fig. 5 where the linear component of the system response is taken out to clearly expose a slightly deformed hysteresis curve. The hysteresis is caused by the relative displacement of the constant magnetic field, generated by the permanent magnet, with respect to the back iron in the actuators. As a result, the magnetic field strength, at any point in the back iron, depends on the orientation of the chopper, and the back iron material exhibits its magnetic hysteresis curve when the mirror is rotated.
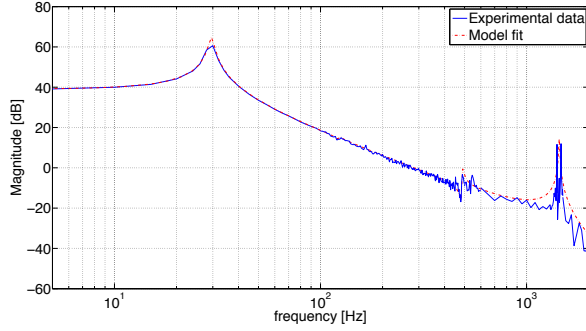
Fig. 3. Bode magnitude plot of θ_x. Experimental data and fitted 8th order model. Experimental data based on sinesweep (Freq. range 5-600 Hz and 1400-1500Hz covered with 5Hz frequency resolution. Other regime covered with 50Hz res.)
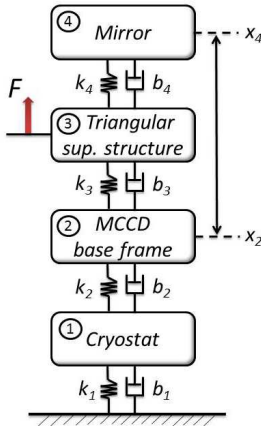
TABLE III
TUNED PARAMETERS OF NON LINEAR MCCD MODEL. NB: THE k_c PARAMETER IS NOT PART OF THE JA MODEL

JA parameters	tuned values	Poly. coef.	tuned values
α	1×10^{-3}	p_1	7.289990×10^{-9}
a	0.44	p_2	2.101289×10^{-9}
k	1750.70	p_3	-2.663815×10^{-6}
c	0.22	p_4	8.192315×10^{-6}
M_s	0.44	p_5	1.059444×10^{-4}
k_c	0.99	p_6	1.608167×10^{-3}

Fig. 4. Non collocated lumped mass system representative for the dominant 8th-order θ_x-dynamics. The actuator force is applied at the triangular support structure and displacements are measured at the mirror surface relative to the MCCD base frame.

The slight deformation of the hysteresis curve is caused by the position dependent reluctance in the magnetic circuit. The reluctance is maximal in the center position ($\theta = 0$) and reduces with increasing angle. This introduces negative magnetic stiffness. As the reluctance of the magnetic circuit is inversely proportional to the magnetic field strength, it also makes the force constant of the actuator position dependent.

In Section III-A we describe the hybrid control method. It includes the design of a feedback controller and of a FF signal. The non linearity has only a small effect on the response of the system and it is not necessary to consider this in the design of the feedback controller. On the other hand, the design of the FF signal is based on a model of the plant. It largely determines the settling time of the mechanism and its performance is directly related to the accuracy of the system model.

In an effort to account for the non linearity in the FF signal design, we included a Jiles-Atherton (JA) hysteresis model [17] in the system description. The JA model is based on physical laws describing the magnetization process in ferromagnetic materials and is thought to be appropriate for the current application. In parallel we added a non linear component in the form of a 5th order polynomial to account

for the deformation of the hysteresis curve. Fig. 6 shows the basic building blocks of the non linear MCCD model. Both operators use the angular orientation of the mechanism as input parameter and affect the input ([N.m]) to the linear plant model.

It is known that tuning the JA model parameters is a difficult process which is strongly dependent on the choice of initial conditions and often results in non ideal solutions [18]. As we have to include 6 extra parameters in our model to also account for the non linearity, related to the positional dependent force constant of the system, tuning of the complete set of parameters becomes even more of a challenge. We tuned the parameters by hand, after which we used Matlabs non linear curve fitting procedure (lsqcurvefit) for fine tuning. This, however, did not result in further optimization of the parameters.

The tuned model parameters are given in Table III. The model response is included in Fig. 5. The fit shows the same characteristic response to a sine input for different amplitudes. The accuracy of the model is however limited. This is supported by the experimental results given in Fig. 7, showing the response of the system to a FF-input applied at different offset positions in the chop range. The FF input was generated on the basis of the linear model and designed to deliver a 1 mrad step. The response of the linear model (blue line) is independent of the offset position in the chop regime while the experimental result clearly shows the dependence on start position, which indicates hysteresis phenomena have taken place. This hypothesis is corroborated by the simulation result when we include the hysteresis model.

The non linear plant model provides valuable insight in the non linear behaviour of the MCCD hardware and fully explains all observed effects. However, from a control design perspective, as the model complexity drastically increases when the hysteresis model (with its 12 parameters) is included, and as the accuracy of the modelled response is limited, we decided not to use the non linear model for the FF design.

III. CONTROL SYNTHESIS

A. Hybrid controller

In this paper we will implement a hybrid controller based on [10], [11]. As the proposed strategy requires switching of the system between feedforward and feedback control, which involves resetting, memorizing and switching between different sets of control states at every start of a scanning period, proof of output regulation is not trivial. The structure
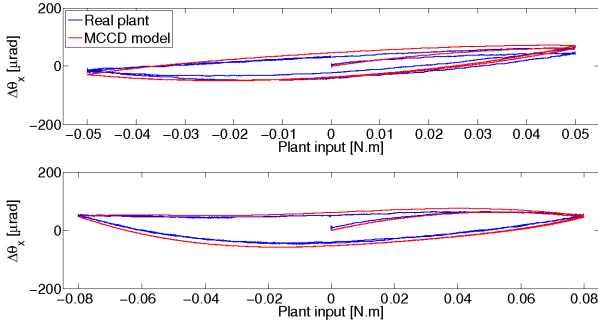
Fig. 5. Observed hysteresis in θ_x and fitted model for sine inputs spanning different parts of the chop range (0.05Nm input corresponds to 4.5 mrad output, 0.08Nm corresponds to 7.2 mrad). Max. displacement (at 0 input) caused by hysteresis is approx. 0.7% of rotated angle. NB: Linear term of system response is taken out to clearly expose the hysteresis.
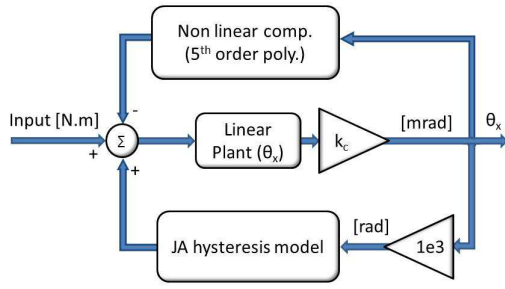

Fig. 6. Non linear MCCD plant model, including a JA model to represent the hysteresis behaviour in the system and an extra non linear term to account for the observed deformation of the hysteresis curve.

of the controller and the results on hybrid output regulation [19] motivated us to formulate the complete system in the hybrid framework. To illustrate this we recall the basic theory from [10], [11].

A hybrid system is a system which exhibits both continues time and discrete time dynamics denoted respectively as flow and jump dynamics. We utilize the hybrid formalism and notation as given in [20].

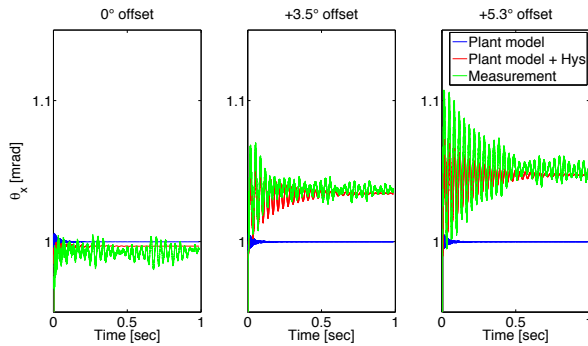**Hybrid system formulation and control design criteria**

Fig. 7. Effect of hysteresis on feedforward response (open loop). Comparison between experiment, linear model and model with hysteresis. Close up at end position for: Left: 0 to +1 mrad step Middle: 3.5 to 4.5 mrad step and Right: 5.3 to 6.3 mrad step. NB: Start position is set to zero in all plots for easy comparison.

For compactness the 1 Degree of Freedom (DoF) dynamics are formulated. Extension to higher dimensions is however trivial as the MCCD is rotationally symmetric and the θ_x and θ_y dynamics are decoupled.

The plant dynamics of the MCCD can compactly be formulated as:

$$\left.\begin{array}{ll} \dot{x} & = A_G x + B_G u, \quad x(t_0) = x_0 \quad \forall (x,u) \in \mathbb{R}^n \times \mathbb{R}, \\ y & = C_G x, \end{array}\right\} \quad (4)$$

Where A_G, B_G and C_G are the state space matrices which realize the transfer function in (3). The input u represents the current input signal to the actuator and the output y is the measured angular displacement.

Observe that by applying u_j to (4) for any arbitrary initial state x_j and initial time t_j, we have

$$x(t_j^+) = M_G x(t_j) + N_j \qquad \forall j \in \mathbb{N}, \quad (5)$$

where the plant transition matrix $M_G := \exp(A_G t_s)$ and

$$N_j = \int_{t_j}^{t_j^+} \exp(A_G(t_j^+ - \lambda)) B_G u_j(\lambda) \, d\lambda.$$

Eq. (5) resembles the jump dynamics in the hybrid system framework. Thus if we apply the input signal u_j at the time interval $t \in [(j+1)t_{obs} + jt_s, (j+1)(t_{obs} + t_s)]$, where t_{obs} defines the length of the observation period between two consecutive steps and t_s is the step time, then the dynamics of the plant can be rewritten in the hybrid systems formulation by first defining the hybrid time domain E as follows:

$$E := \bigcup_{j=\mathbb{N}} [jt_{obs}, (j+1)t_{obs}] \times \{j\}.$$

The dynamics of x on E can equivalently be described by the following hybrid system

$$\left.\begin{array}{ll} \dot{\tau}_c & = 1 \\ \dot{\zeta} & = A_G \zeta + B_G v, \quad \zeta(0,0) = \zeta_0 \\ & \forall (\tau_c, \zeta, v) \in [0, t_{obs}] \times \mathbb{R}^n \times \mathbb{R} \\ \\ \tau_c^+ & = 0 \\ \zeta^+ & = M_G \zeta + N_j \quad \forall (\tau_c, \zeta) \in t_{obs} \times \mathbb{R}^n \\ y & = C_G \zeta, \end{array}\right\} \quad (6)$$

where $\zeta_0 = x(0)$, v is the additional control signal applied during the flow periods and τ_c is a clock variable with a dwell time t_{obs} which defines the moment of jumping of the system.

This reformulation of the plant dynamics into hybrid setting opens the possibility of assigning optimal control solutions during the first t_s seconds (which are computed off-line for the nominal positions) and implementing a hybrid feedback controller to stabilize the system.

Following the hybrid output regulation setting as in [19], we can adopt the following exosystem which generates the reference signal r and is also defined on the hybrid time domain E as above

$$\left.\begin{array}{ll} \dot{\tau}_c & = 1 \\ \dot{w} & = Sw, \quad w(0,0) = w_0 \quad \forall (\tau_c, w) \in \mathcal{W} \\ \\ \tau_c^+ & = 0 \\ w^+ & = Jw \quad \forall (\tau_c, w) \in \mathcal{W} \cap (\{t_{obs}\} \times \mathbb{R}^s) \\ r & = Qw, \end{array}\right\} \quad (7)$$

with

$$S = \begin{bmatrix} \Upsilon & 0 \\ 0 & 0 \end{bmatrix}_{(4q \times 4q)} \quad \Upsilon = \begin{bmatrix} 0 & \omega_n & 0 & 0 \\ -\omega_n & 0 & 0 & 0 \\ 0 & 0 & 0 & 1 \\ 0 & 0 & 0 & 0 \end{bmatrix}$$

$$J = \begin{bmatrix} 0 & I_{(4*(q-1))} \\ M_e^{-1} & 0 \end{bmatrix} \quad M_e = \exp(\Upsilon * t_{obs})$$

$$Q = \begin{bmatrix} 1 & 0 & 1 & 0 & 0_{(1 \times (4(q-1)))} \end{bmatrix}$$

and

$$w = \begin{bmatrix} w_1 & w_2 & \dots & w_q \end{bmatrix}$$
$$w_p = \begin{bmatrix} w_{p1} & w_{p2} & w_{p3} & w_{p4} \end{bmatrix}.$$

Finally $\mathscr{W} := \{(\tau_c, w) : \tau_c \in [0, t_{obs}], w \in W(\tau_c)\}$, where the set valued mapping $\tau_c \to W(\tau_c) \subset \mathbb{R}^s$ is continuous with compact values. The parameter $q \in \mathbb{N}$ defines the number of integration periods that constitute a single repetition of the reference profile. $p \in \{1, 2, \dots, q\}$ and ω_n is the angular velocity of the oscillator. The matrix M_e is the transition matrix related to Υ. The presence of the inverse of this term in the jump matrix J guarantees that the active exo-state variables are reset to their initial value after every period of flow, even if $t_{obs} \neq 2\pi/\omega_n$.

The exosystem can generate all astronomical observation modes that are discussed in [3], except for spiral chopping, by choosing the appropriate initial conditions $w_0 := w(0, 0)$ in combination with the required form of N_j to jump between the different flow sets.

NB: For the current application we only consider square wave chopping which greatly simplifies the exosystem description. We present the full description here to illustrate the necessity to reset the control states at the end of each flow period. For square wave chopping ($q = 2$) the matrices can be reduced to the following form:

$$S = \begin{bmatrix} 0 & 0 \\ 0 & 0 \end{bmatrix} \quad J = \begin{bmatrix} 0 & 1 \\ 1 & 0 \end{bmatrix} \quad Q = \begin{bmatrix} 1 & 0 \end{bmatrix} \quad (8)$$

Based on this exosystem description and applying the internal model principle as in [19], the hybrid controller can now be described in the following way

$$
\left.
\begin{aligned}
\dot{\tau}_c &= 1 \\
\dot{\xi} &= A_C \xi + B_C e, \quad \xi(0, 0) = \xi_0 \\
&\quad \forall (\tau_c, \xi, e) \in [0, t_{obs}] \times \mathbb{R}^m \times \mathbb{R} \\
\tau_c^+ &= 0 \\
\xi^+ &= \Phi \xi + \Psi e \\
&\quad \forall (\tau_c, \xi, e) \in \{t_{obs}\} \times \mathbb{R}^m \times \mathbb{R} \\
v &= C_C \xi + D_C e
\end{aligned}
\right\}
\quad (9)
$$

where

$$A_C = \begin{bmatrix} \star & 0 \\ 0 & S \end{bmatrix}$$

$$B_C = \begin{bmatrix} \star & k_1 & 0 & k_2 & k_3 & 0_{(1 \times (4(q-1)))} \end{bmatrix}^T$$

$$C_C = \begin{bmatrix} \star & Q \end{bmatrix} \quad D_C = \begin{bmatrix} \star \end{bmatrix}$$

$$\Phi = \begin{bmatrix} I_\star & 0 \\ 0 & J \end{bmatrix} \quad \Psi = \begin{bmatrix} \star \\ 0 \end{bmatrix},$$

the parameters k_1, k_2 and k_3 are controller gains. The elements in $\star$ are related to the design of a robust feedback controller and can be designed according to each different application. The identity matrices in Φ indicate that the states related to $\star$ are not changing as a result of the jump. The J in the ϕ matrix is identical to the jump matrix of the exosystem. Again the inverse of M_e guarantees that in the steady state, the active control states related to the internal model jump back to the correct initial state at the end of the flow period. The variable e is the error signal, i.e., $e = r - C_G \zeta$. Again this general form can be reduced to the special case of square wave chopping by applying (8) and reformulating the input matrix as $B_C = \begin{bmatrix} \star & k_1 & 0 \end{bmatrix}^T$.

Finally, the complete closed loop hybrid system is given by:

$$
\left.
\begin{aligned}
\dot{\tau}_c &= 1, \quad \dot{w} = Sw, \quad w(0, 0) = w_0 \\
\begin{bmatrix} \dot{\zeta} \\ \dot{\xi} \end{bmatrix} &= \mathscr{H}_{cl} \begin{bmatrix} \zeta \\ \xi \end{bmatrix} + \mathscr{L}_{cl} w, \quad \begin{bmatrix} \zeta(0,0) \\ \xi(0,0) \end{bmatrix} = \begin{bmatrix} \zeta_0 \\ \xi_0 \end{bmatrix} \\
&\quad \forall ((\tau_c, w), \zeta, \xi) \in \mathscr{W} \times \mathbb{R}^n \times \mathbb{R}^m \\[4pt]
\tau_c^+ &= 0, \quad w^+ = Jw \\
\begin{bmatrix} \zeta^+ \\ \xi^+ \end{bmatrix} &= \mathscr{J}_{cl} \begin{bmatrix} \zeta \\ \xi \end{bmatrix} + \mathscr{M}_{cl} w \\
&\quad \forall ((\tau_c, w), \zeta, \xi) \\
&\quad \in (\mathscr{W} \cap (\{t_{obs}\} \times \mathbb{R}^s)) \times \mathbb{R}^n \times \mathbb{R}^m
\end{aligned}
\right\}
\quad (10)
$$

with

$$\mathscr{H}_{cl} := \begin{bmatrix} A_G - B_G D_C C_G & B_G C_C \\ -B_C C_G & A_C \end{bmatrix} \quad \mathscr{L}_{cl} := \begin{bmatrix} B_G D_C Q \\ B_C Q \end{bmatrix}$$

$$\mathscr{J}_{cl} := \begin{bmatrix} M_G & 0 \\ -\Psi C_G & \Phi \end{bmatrix} \quad \mathscr{M}_{cl} := \begin{bmatrix} N_{w_j} \\ \Psi Q \end{bmatrix}$$

where N_j is related to the exo-state through N_{w_j}, i.e., $N_j := N_{w_j} w$.

Based on this reformulation of the plant dynamics in the hybrid system framework, we can define the chopper scanning control problem as follows:

Chopper scanning hybrid control problem: Design a hybrid controller (9) for the hybrid plant (6) such that the closed-loop system (10) has bounded trajectories and $\lim_{t+j \to \infty} e(t, j) = 0$ uniformly.

The following result defines necessary and sufficient conditions to solve the chopper scanning hybrid control problem.

This can be used for synthesis of the hybrid controller with the considered plant dynamics.

Let ϕ_{cl} be the state transition matrix of the flow dynamics

$$\begin{bmatrix} \dot{\zeta} \\ \dot{\xi} \end{bmatrix} = \mathscr{H}_{cl} \begin{bmatrix} \zeta \\ \xi \end{bmatrix}.$$

In other words $\phi_{cl}(t_{obs}) = \exp(\mathscr{H}_{cl} t_{obs})$ and $\phi_{cl}(t_0) = I_{n+m}$.

Proposition 3.1: Assume that the restriction of $\mathscr{H}_{cl}$ to the active subspace is Hurwitz. Then there exists an attractive invariant manifold $\mathscr{M}$ such that $Qw - C_G\zeta = 0$ if and only if

$$\gamma := \left| \sigma_{\max} \left(\prod_{h=0}^{l-1} \mathscr{J}_{cl_{(l-h)}} \phi_{cl}(t_{obs_{(l-h)}}) \right) \right| < 1, \qquad (11)$$

where $\sigma_{\max}$ is the largest eigenvalue of the matrix and l is the number of scans contained in the smallest repeating sequence of scans with different t_{obs}. In particular, we have that $e = r - C_G\zeta \to 0$ as $t + j \to \infty$.

If we satisfy condition (10), the plant asymptotically converges to the invariant manifold which satisfies zero error tracking (this also implies a bumpless transition when switching between feedforward and feedback control).

For a detailed description of the hybrid control method and for the proof of output regulation the reader is referred to [10], [11].

A typical timeline for square wave chopping, applying the hybrid control strategy, is given in Figure 9. Indicated are the periods where feedforward or feedback control is applied. The arrows visualize the reset and memory actions.

Simulation results of MbFF vs hybrid stepping

To illustrate why we perform the step in open loop, we simulated the effect of the step time of the reference profile on the settling time of a second order plant for the MbFF and the hybrid strategy. For completeness we also included the result when applying the feedback loop without the FF path. The FF signal is based on an inverse plant model which exhibits frequency dependent inaccuracies. We applied a PID controller which was tuned for a certain bandwidth and limited overshoot of the closed loop plant. The different configurations studied are summarized in Table IV. For clarity the effect of noise and disturbances is excluded from the results as, for the field of nano positioning, this will typically affect the positional stability of the plant before it has a significant effect on settling time. Plant constraints are not considered in the simulation.

Figure 8 shows the results of the simulations. The hybrid controller outperforms the MbFF for fast reference profiles. For slower reference profiles the closed loop improves the tracking of the reference and the MbFF approach shows slightly better results. As can be expected, increasing the closed loop bandwidth reduces the settling time.

The results vary with every specific configuration, but generally speaking it can be concluded that for fast reference profiles, with respect to the typically limited controller bandwidth, open loop stepping performs better.

Design of FF input u_j

TABLE IV
PLANT CONFIGURATIONS STUDIED TO ILLUSTRATE THE EFFECT OF REFERENCE STEP TIME ON SETTLING. CONFIGURATIONS 1 AND 2 REPRESENT A CRITICALLY DAMPED PLANT. THE FF SIGNAL IS BASED ON A PLANT MODEL INVERSE WITH HIGH FREQUENCY INACCURACIES MODELLED BY A 1000 RAD/SEC BW. LOW PASS FILTER. CONFIGURATIONS 3 AND 4 DESCRIBE A PLANT WITH A RESONANCE. THE MODEL MISMATCH IS IN THE LIMITED REPRESENTATION OF THE RESONANCE. FOR BOTH SCENARIOS PID CONTROLLERS ARE TUNED WITH DIFFERENT CL. BANDWIDTHS.

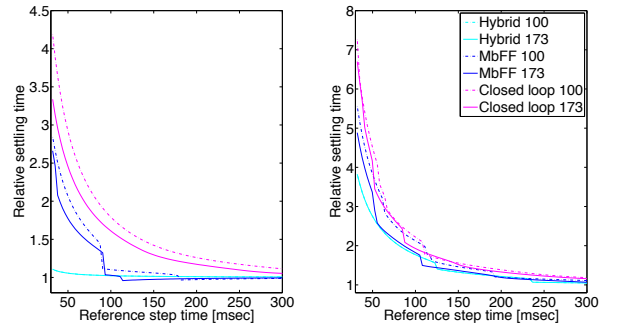|	Plant	Inverse plant model	PID parameters	Cl. bw. [rad/sec]
1	$\frac{10^4}{s^2+2\times10^2 s+10^4}$	$\frac{10^2 s^2+2\times10^4 s+10^6}{s^2+2\times10^3 s+10^6}$	$k_p=2$ $k_i=102$ $k_d=9.83\times10^{-3}$	100
2			$k_p=3.47$ $k_i=173$ $k_d=1.73\times10^{-2}$	173
3	$\frac{10^4}{s^2+10^2 s+10^4}$	$\frac{10^6 s^2+1.2\times10^8 s+10^{10}}{s^2+2\times10^5 s+10^{10}}$	$k_p=1.12$ $k_i=81.5$ $k_d=3.85\times10^{-3}$	100
4			$k_p=2.57$ $k_i=137$ $k_d=1.21\times10^{-2}$	173

Fig. 8. Effect of step time of reference profile on settling time of system configurations given in Table IV for the hybrid, MbFF and closed loop only control strategies (Left: results for conf. 1 and 2. Right: results for conf. 3 and 4). The relative settling is defined as the settling time of the plant normalized by the applied reference step time. The Hybrid 100 and 173 results largely overlap because of the limited influence of the PID controller after the step (as a result of the very small error signal).

The FF signal is generated by applying quadratic programming to the following optimization problem with input constraints

$$\min_{u_j \in U} \| x_d(t_s) - x(t_s) \|_2 \qquad (12)$$

where U is the set of allowed control inputs $U := \{u_j \in \mathbb{R}^n : |u_{j_i}| \leq 4.2\text{N.m}\}$, $x_d(t_s)$ is the desired plant state at the end of the step (at time t_s) and $x(t_s)$ is the realized end state as a result of the discrete FF input sequence. This approach can handle input constraints and deals with the discrete nature of the FF input naturally.

We recognize that, because of the high frequency reference signal in relation to the typically limited bandwidth of the closed loop controller, fast settling can only be achieved by accurate FF design and not by error convergence after switching to closed loop. Therefore, we use the full 5 msec settling time specification for our FF signal. This maximizes
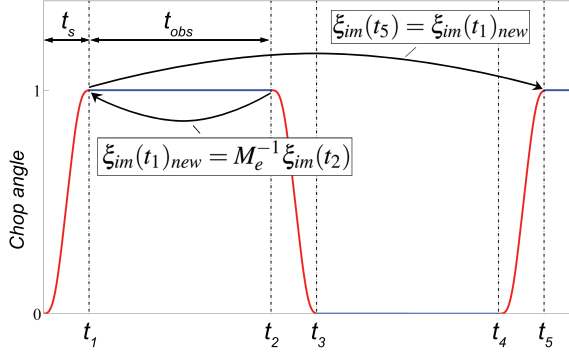
Fig. 9. Chopping timeline (first repetition only). The step (red curve) is performed applying FF only (u_j). During the observation periods (blue curve) the hybrid controller is active (v). The reset and memory actions are visualized by the arrows. The control states related to the internal model (ξ_{im}) are reset at time t_2 to the corresponding values at t_1. These states are applied as initial condition during the next repetition at the same observation position. (The same applies to the second observation position).

TABLE V
INFLUENCE OF PLANT RESONANCES ON SETTLING WHEN APPLYING A FF SIGNAL BASED ON THE 2nd-ORDER PLANT MODEL FOR A STEP FROM $\theta_x=0$ TO 8.5 MRAD. THE RESONANCES CONSIDERED IN THE DIFFERENT PLANT MODELS ARE GIVEN IN THE TABLE. NB: THE COMPLETE 8th-ORDER PLANT ALSO SETTLES WITHIN 4.9 MSEC WHEN APPLYING A FF SIGNAL BASED ON THE 8th-ORDER PLANT MODEL.

Plant model	Overshoot [μrad]	Settling [msec]
2nd-order (30Hz)	0	4.9
4th-order (30Hz+125Hz)	29	320
4th-order (30Hz+500Hz)	11	72
4th-order (30Hz+1500Hz)	23	80
Complete 8th-order	61	320

the number of individual discrete steps of the FF which allows for better norm reduction of (12) and it reduces the maximum forces exerted on the mechanism. The effect of which is the reduction of resonant behaviour after the step as a result of model uncertainties and non modelled dynamics. Furthermore, as this also limits the peak currents generated by the amplifier, this gives the possibility to reduce the amplifier output range. As reduction of the amplifier range typically means reduction of the amplifier noise levels, this has a direct positive effect on the positional stability of the mechanism.

Table V summarizes the result of a simulation where we applied an accurately designed FF signal based on the 2nd-order MCCD plant model (including only the 29.6Hz rigid body mode) to different model plant configurations. This clearly shows the necessity to include the higher order resonances in the FF-design.

Feedback controller

The feedback controller for θ_x has been tuned by loop shaping. It consists of a skew notch filter, to compensate the large phase shift introduced by the dominant resonance at 29.6 Hz, an integrator, required for constant reference tracking and a first order low pass filter for high frequency cut off. The complete controller, discretized by the Tustin method, is then

given by:

$$C_{\theta_x} = \frac{0.1722z^4 - 0.3337z^3 - 0.01048z^2 + 0.3337z - 0.1617}{z^4 - 3.311z^3 + 4.085z^2 - 2.228z + 0.4531}$$

In Fig. 10, the bode plot of both the sensitivity function $S = (1+PC)^{-1}$ and the complementary sensitivity function $T = PC(1+PC)^{-1}$ of the closed loop plant are given. T shows good tracking ability at low frequencies. S was tuned for sufficient amplifier noise and disturbance attenuation below 100 Hz. The slight peaking of the Bode magnitude plot of S above 200 Hz (max. of 4dB at 500Hz) is allowed because of the low sensor noise in the system. The gain and phase margins of the closed loop system are respectively 14.3 dB and 82°, from which we can conclude that the feedback loop is robustly stable. The value of γ, as defined in (11), is 0.36, so we satisfy the necessary and sufficient condition for output regulation of the hybrid controller.

Because of the symmetry in the system, and because we do not specifically shape the 125Hz and 487Hz resonances, the same controller can be applied to the θ_y DoF. For the control of the z-displacement it suffices to apply a discrete PID controller with $k_p = 89$, $k_i = 1000$ and $k_d = 0.56$ with a 4012.6 filter bandwidth (Forward Euler discretization method).
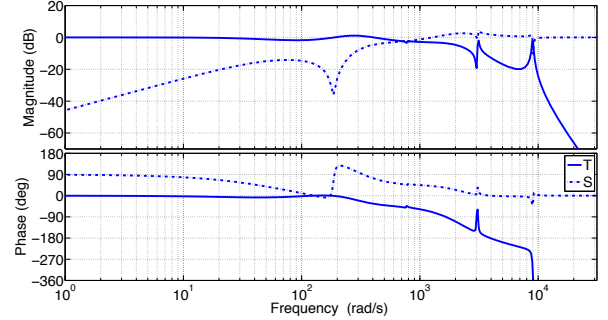

Fig. 10. Bode plot of complementary sensitivity (T) and sensitivity function (S) of closed loop plant for θ_x.

B. Repetitive controller

Fig. 11 shows the repetitive control layout. The repetitive loop is placed in parallel with the feedback controller described in Section III-A. The repetitive loop consists of a so called L-filter for phase compensation, a Q-filter to add robustness and an internal model which can generate any repetitive signal with period N.

The learning update law of the repetitive loop can be formulated as follows:

$$z^N U_r(z) = Q(z)(U_r(z) + z^\gamma L(z)k_r E(z)), \qquad (13)$$

where $z^N U_r(z)$ is the new input which will be applied during the next repetition and is constructed from the input of the current repetition $U_r(z)$ and from the error $z^\gamma E(z)$ as a result of this input. From the feedback loop we have

$$E(z) = -S_p(z)U_r(z), \qquad (14)$$

where $S_p = P/(1 + PC)$ is the plant sensitivity function. Combining (13) and (14) gives us

$$z^N E(z) = Q(z)(1 - z^\gamma S_p(z)k_r L(z))E(z),$$

which can be interpreted as the error propagation with every repetition, from which it can directly be concluded that the error converges monotonically if $|Q(1 - z^\gamma S_p k_r L)| < 1$ for all frequencies up to the Nyquist frequency. Taking $L = S_p^{-1}$, $k_r = 1$ and $\gamma = 0$ theoretically delivers perfect tracking after only one iteration (dead-beat solution). However, an exact inverse is typically not realizable as the inverse of S_p often is non proper or even unstable as a result of respectively a proper or non minimum phase S_p. Different techniques, such as ZPETC [21], are available for the design of L, but the match is typically not exact and plant uncertainties and non modelled dynamics further limit the accuracy of the filter design. The lead term z^γ can be used to partly compensate for the phase lag introduced by the non ideal L-filter as described in [9]. The Q-filter can be designed as a low pass filter to allow for monotonic error convergence but this comes at the cost of reduced tracking performance.

The reproducibility is generally considered to be a measure for the tracking accuracy that can be attained by repetitive control. The reproducibility of the MCCD for chopping is $\Delta\theta < 10\mu$rad during the step and $\Delta\theta < 2\mu$rad during the integration periods.

In our experiment, as we are interested to explore the maximum settling performance using the repetitive method, we take $Q = 1$. This allows for maximum error reduction at the cost of monotonic convergence. We avoided inversion of S_p but used an inverse of the 4th-order θ_y-dynamics of the plant as our L-filter, where we added a 4th-order Butterworth filter to make the transfer function proper. We are aware that sampling of a continuous time system may lead to the introduction of RHP zeros in the discrete model [22], which in turn can cause problems during system inversion. To avoid this problem we designed the filter in continuous time, after which the L-filter was discretized by the Tustin method. The resulting filter is then given by:

$$L = \frac{0.048z^4 + 6.253e - 5z^3 - 0.096z^2 - 2.939e - 5z + 0.048}{z^4 - 3.187z^3 + 3.876z^2 - 2.124z + 0.441}.$$

To avoid interference between the feedback controller and the repetitive loop we only close the loop after convergence of the repetitive controller.

Because of the good match between the model and the hardware, we could tune k_r, γ and the cut off frequency of the Butterworth filter offline, and no adjustments of the parameters were needed when we applied the method to the real hardware. NB: The good quality of the learned step input does not introduce significant oscillations after the step. This and the large stability margins of the feedback loop, allowed us to further increase the gain of the feedback controller for better amplifier noise and disturbance attenuation. The tuned parameters are given in Table VI. The gain of the feedback controller was increased by a factor of 1.5.

The reference profile for chopping is generated by applying the method described in [23]. This method generates a smooth

TABLE VI
TUNED PARAMETERS FOR REPETITIVE CONTROLLER FOR θ_x AND θ_y.

DoF	k_r	γ	Cut off freq. [Hz]
θ_x	0.1	8	500
θ_y	0.5	9	500

4th-order reference profile while taking into account the limits (maximum jerk etc.) of the plant.

In Fig. 12 the good match between the simulation and the experimental results is shown. After about 2.4 seconds (12 iterations) the repetitive controller has converged. The effect of activating the feedback controller after 4.7 seconds is clearly visible.

The compensator for θ_x is very similar but here the resonances of the L-filter are matched with the 29.6Hz and 1440Hz resonances of P_{θ_x}.
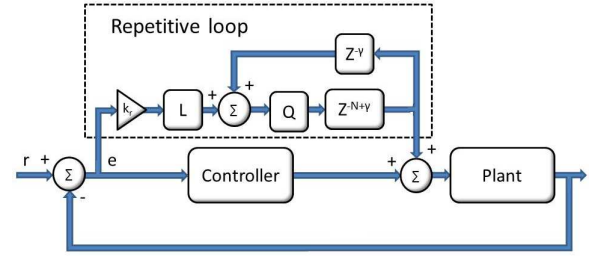

Fig. 11. Repetitive control layout. The repetitive loop is placed in parallel with the standard feedback controller. N is the number of discrete samples in one repetition.
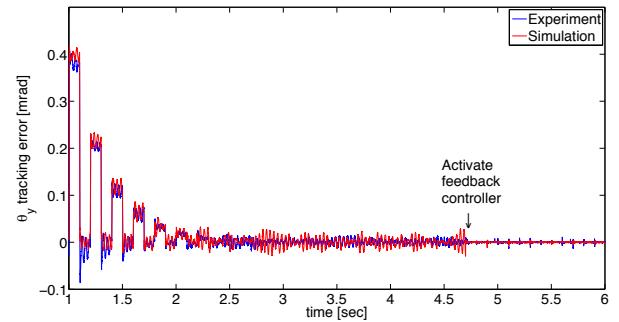

Fig. 12. Comparison of simulation result with experiment when tracking a 5Hz chopping reference between 0 and 8.5 mrad in θ_y. Error convergence from 1 sec onwards is shown. Feedback controller is activated after 4.7 sec.

We use a practical approach for our repetitive controller design to be able to study its general performance without the need for S_p inversion of the high order plant described in Table II. We are aware that small changes in the response can occur when applying a (zero phase) Q-filter and inversion of S_p. However, for θ_y the tracking error is in the order of the reproducibility of the system which means that for this DoF no further improvements can be made. The performance of the repetitive controller is discussed in Section IV. Some considerations about the implementation of the method on the final MCC hardware are discussed in Sections V and VI.

IV. Experimental results

All tests are performed with the test setup as described in Section *II.A*. Table VII summarizes the most important test results. All results, except for the settling time are generated applying the hybrid controller. As we use the same feedback controller, most results are applicable to both control strategies. It is well known that the influence of stochastic disturbances (system noise and external vibrations) are amplified by the repetitive method [24]. Because of this the positional stability is worse than for the hybrid approach. However, as discussed in Section *III.B*, we could compensate for this effect by increasing the loop gain of the feedback controller.

Most requirements are satisfied but the positional stability specification and the settling time are not fully met. We believe that the positional stability can be further improved by fine tuning of the feedback controller in the final setup (when the exact noise and disturbance levels on the E-ELT platform are known), and by reduction of the amplifier range as discussed in Section III-A. In [25] the effectiveness of different strategies to reduce the negative influence of stochastic disturbances on positional stability when applying a repetitive controller is investigated. If required this approach can be considered to further reduce the influence of stochastic disturbances on the positional stability of the plant.

The settling time results given in Table VII are generated by the repetitive controller. Fig. 13 shows the result of chopping in θ_y between 0 and 8.5 mrad for both the hybrid and repetitive method. The hybrid controller converges within 1 chop cycle. The repetitive controller takes about 9 cycles but the settling time is much better. This is illustrated in Fig. 14 where a close up of the settling behaviour at the 8.5 mrad position after convergence is given. Since an observation typically takes minutes, the time required for learning (approx. 2 sec) is easily compensated by the much better settling performance of the repetitive controller.

As discussed in Section *II.C*, the quality of the FF signal applied in the hybrid method is limited as a result of the non modelled non linearities in the system. This limits the performance of any model based FF method. As argued in [9], the linear repetitive controller can deal with the small non linearity in the system and there is no need for adding extra complexity by applying a non linear repetitive controller.

The difference in the settling time for θ_x and θ_y can be explained by the resonant behaviour of the experimental setup at approximately 500Hz, which is only present in the θ_x-dynamics. Including the modelled resonance at 500Hz in the L-filter design for θ_x did not improve performance because of the limited accuracy of the modelled resonance. More detailed modelling is required to correctly compensate for this effect in the *L*-filter design, but, as the resonance is part of the test setup and not of the MCCD hardware, we did not put further effort into solving this issue. Instead the issue was taken up with the design engineers of the METIS team recommending to avoid low frequency resonances in the structural interface of the MCC with the METIS instrument.

When applying the repetitive controller we ignored the typical design rule of monotonic error convergence ($|Q(1 -$
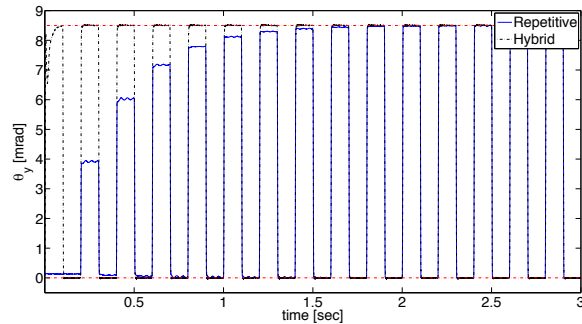

Fig. 13. Experimental result of 5Hz chopping in θ_y between 0 and 8.5 mrad, applying the hybrid and the repetitive controller.
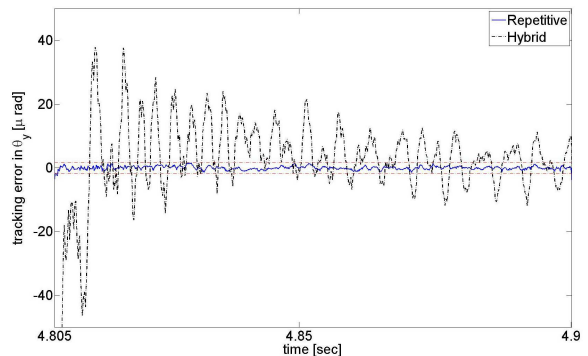

Fig. 14. Tracking error during 5Hz chop after convergence (after 4.805 sec at θ_y= 8.5 mrad position). Tracking of the hybrid controller is limited due to the non linearities which are not accounted for in the FF design.

$z^\gamma S_p k_r L)| < 1$), in order to maximize the learning bandwidth. Monotonic convergence is very important for the delicate hardware, but the necessary use of a Q-filter will limit the learning bandwidth of the repetitive controller. The realizable learning bandwidth strongly depends on the quality of the system identification and the ability of the L-filter to compensate for the resonances within the required learning bandwidth. If for the final hardware fast settling can only be achieved while ignoring the rule of monotonic convergence, the repetitive method will be used to generate a satisfactory FF-signal, after which the learning is switched off. This FF-signal can then be applied to either the MbFF or the hybrid approach. As

TABLE VII
MCCD REQUIREMENTS AND REALIZED PERFORMANCE. POSITIONAL
STABILITY IS DEFINED AS $3\times$ RMS (σ) LEVEL, ALL OTHER
REQUIREMENTS ARE DEFINED AS ABSOLUTE MAXIMUM.

Description	Requirement	Result	Unit	Remark
Pos. stability	≤ 1.7	≤ 2.09	[μrad]	3σ
Pos. repeatability	≤ 1.7	≤ 0.4	[μrad]	
Pos. accuracy	≤ 85	≤ 1.04	[μrad]	
Settling time in θ_x	≤ 5	32	[msec]	applying
Settling time in θ_y	≤ 5	5.6	[msec]	rep. control
Parasitic z-disp.	≤ 200	≤ 3	[μm]	
Power dissipation	< 1	0.116	[W]	for 5Hz chop
Peak currents	≤ 10	2.75	[A]	over 8.5 mrad
Thermal stability	≤ 1.7	< 1.7	[μrad]	

discussed in Section III-A, which one to choose will depend on the final system configuration.

We tested this scenario in simulation on the non linear MCCD model by first applying the repetitive controller to the plant for a 0 to 8.5 mrad chop sequence. The repetitive method generates an FF signal which we then used as the FF input for both the MbFF and hybrid control strategies. A close up of this simulation at the 8.5 mrad position after 10 seconds of chopping is given in Fig. 15. The different methods show comparable step results, which can be explained by the high accuracy of the FF signal (small positional errors during the step and accurate end position).
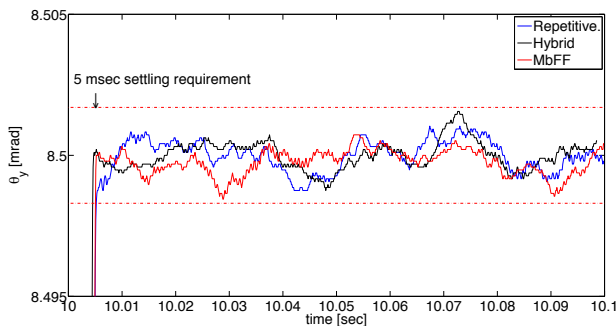
Fig. 15. Simulation of 5Hz chopping between 0 and 8.5 mrad on the non linear plant, applying the repetitive, MbFF and hybrid controller all using the FF-signal learned by the repetitive method. Close up at 8.5 mrad position. Result after convergence of the repetitive controller and switching to closed loop. Red dotted lines indicate 1.7 μrad positional stability limits.

V. Conclusions

We tested the performance of the MCCD applying a new hybrid control strategy and compared the results to those when using a repetitive controller. The hybrid control strategy has been developed to eliminate the typical negative effect of the closed loop controller on settling when tracking fast reference profiles applying the standard MbFF technique. Simulation results presented in Section III-A show that for the considered plant uncertainties, the hybrid method out performance the MbFF technique when fast reference signals are applied.

Detailed system identification revealed the presence of non negligible non linearities in the mechanism. The developed non linear plant model clearly explains the observed non linear behaviour of the plant. Accurate tuning of the non linear system parameters is however difficult, and the approach was considered to be too complex for implementation in the final hardware. This limits the performance of any MbFF approach (including the proposed hybrid controller).

The results of the repetitive controller are very promising. We applied an open loop learning approach to show the possible performance of the repetitive control strategy without the need for S_p inversion. The repetitive controller can handle the non linearities in the plant. When chopping in the θ_y-direction we reach the reproducibility limit of the system, which means that we make maximum use of its capabilities.

As the repetitive method is a well established control strategy with a firm mathematical background, and as it has shown its applicability to the hardware, this control strategy will be applied to the final MCC mechanism. If satisfying monotonic convergence limits the settling performance, the repetitive method will be used for learning of the FF-signal offline after which this FF can be applied to the MbFF or hybrid method.

The performed test program concludes the METIS Cold Chopper Demonstrator project. Because of the very promising results when applying the repetitive controller it was decided not to change the MCC design significantly for the final hardware. This means no reduction of hysteresis in the actuators. We believe that detailed tuning of the feedback controller in the final setup, and limiting the amplifier range will suffice to meet the positional stability requirement. Recommendations concerning the allowed resonance spectrum of the mechanical interface of the MCCD with the METIS instrument were provided to the METIS design team.

References

[1] B.R. Brandl *et.al.* "METIS: the mid-infrared E-ELT imager and spectrograph," Proc. SPIE, 9147, Ground-based and Airborne Instrumentation for Astronomy V, 914721, 8, 2014; doi:10.1117/12.2056468.

[2] European Southern Observatory, "E-ELT instrument roadmap," The E-ELT construction proposal, ESO, C4: 3-32, 2012.

[3] A. Kovács, "Scanning strategies for imaging arrays," Proc. SPIE, 7020, 5, 2008

[4] M. Boerlage, M. Steinbuch, P.F. Lambrechts and M. van de Wal, "Model based feedforward for motion systems," Proc. IEEE int. conf. on control applications (CCA), Istanbul, Turkey, pp. 11581163, 2003.

[5] D.E. Torfs, R. Vuerinckx, J. Swevers and J. Schoukens, "Comparison of two feedforward design methods aiming at accurate trajectory tracking of the end point of a flexible robot arm," IEEE Transactions on Control Systems Technology, 6(1), 114, 1998.

[6] W. Singhose, "Command shaping for flexible systems: A review of the first 50 years," Int. J. Precision Eng. Manuf., vol. 10, no. 4, pp. 153168, 2009.

[7] W. Singhose and J. Vaughan, "Reducing vibration by digital filtering and input shaping," IEEE Transactions on control systems technology, VOL. 19, NO. 6, NOVEMBER 2011

[8] C. Li, D. Zhang and X. Zhuang, "A survey of repetitive control," Proc. of 2004 IEEE/RSJ International Conference on Intelligent Robots and Systems, Sendai, Japan, pp. 11601166, 2004.

[9] R.W. Longman, "Iterative learning control and repetitive control for engineering practice," Int. J. Contr., vol. 73, no. 10, pp. 930954, 2000.

[10] R. Huisman, J. Boomer and B. Jayawardhana "Hybrid control synthesis for output regulation with applications to fast motion nano-positioning mechanisms," under review

[11] R. Huisman and B. Jayawardhana, "On the design of hybrid output regulation for the METIS cold chopper," Proc. 7th IFAC Symposium on Robust Control Design, Aalborg, 2012.

[12] D. Roover and F. Sperling, "Point-to-point control of a high accuracy positioning mechanism," Proc. American Control Conf. Albuquerque, U.S.A., pp. 13501354, 1997.

[13] J.C. Clegg. A nonlinear integrator for servomechanisms. Transactions of the American Institute of Electrical Engineers, 77 (Part II): 41-42, 1958.

[14] T. Tuma, A. Pantazi, J. Lygeros and A. Sebastian. Nanopositioning with impulsive state multiplication: A hybrid control approach. IEEE Transactions on Control Systems Technology, 21.4: 1352-1364, 2013.

[15] S. Paalvast, et al. "Development and characterization of a 2D precision cryogenic chopper for METIS," SPIE Astronomical Telescopes+ Instrumentation. International Society for Optics and Photonics, 2014.

[16] M. Eggens, "Results analysis METIS chopper mirror surface deformation," MCCD project documentation, Doc: SRON-MCCD-RP-2011-00, 2011.

[17] D. C. Jiles and D. L. Atherton, "Theory of ferromagnetic hysteresis," J. Magn. Magn. Mater., vol. 61, pp.48 -60 1986.

[18] D. Lederer, H. Igarashi, A. Kost and T. Honma, "On the parameter identification and application of the Jiles-Atherton hysteresis model for numerical modelling of measured characteristics," IEEE Trans. Magn., vol. 35, pp. 1211-1214, 1999

[19] L. Marconi and A.R. Teel. A note about hybrid linear regulation. In 49th IEEE Conference on Decision and Control, pages 1540-1545, Atlanta, Georgia, 2010.

[20] R. Goebel, R.G. Sanfelice and A.R. Teel. Hybrid dynamical systems. IEEE Control Systems Magazine, 29: 28-93, 2009.

[21] M. Tomizuka, "Zero phase error tracking algorithm for digital control," ASME Journal of Dynamic Systems, Measurement and Control, 109:6568, 1987.

[22] K.J. Åström, P. Hagander and J. Sternby. "Zeros of sampled systems," Automatica 20(1): 31-38, 1984.

[23] P.F. Lambrechts, M. Boerlage and M. Steinbuch, "Trajectory planning and feedforward design for high performance motion systems," Proc. American Control Conf. Boston, U.S.A., pp. 4637-4642, 2004.

[24] R.J.E. Merry, M.J.G. van de Molengraft and M. Steinbuch, "Disturbances and model uncertainties in iterative learning control," Proc. 4th int. workshop on multidimensional systems (NDS), pp. 136-141, 2005.

[25] M. Butcher, A. Karimi and R. Longchamp, "A statistical analysis of certain iterative learning control algorithms," International Journal of Control, 81(1) pp. 156166, 2008